A&A 501, 89–102 (2009)
DOI: 10.1051/0004-6361/200811284

Astronomy & Astrophysics

The X-ray view of giga-hertz peaked spectrum radio galaxies

O. Tengstrand[1,2], M. Guainazzi[1], A. Siemiginowska[3], N. Fonseca Bonilla[1], A. Labiano[4], D. M. Worrall[5], P. Grandi[6], and E. Piconcelli[7]

[1] European Space Astronomy Centre of ESA, PO Box 78, Villanueva de la Cañada, 28691 Madrid, Spain
e-mail: Matteo.Guainazzi@sciops.esa.int
[2] Institute of Technology, University of Linköping, 581 83 Linköping, Sweden
[3] Harvard-Smithsonian Centre for Astrophysics, 60 Garden St., Cambridge, MA 02138, USA
[4] Departamento de Astrofísica Molecular e Infrarroja, Instituto de Estructura de la Materia (CSIC), Madrid, Spain
[5] H. H. Wills Physics Laboratory, University of Bristol, Tyndall Avenue, Bristol BS8 1TL, UK
[6] Istituto di Astrofisica Spaziale e Fisica Cosmica-Bologna, INAF, via Gobetti 101, 40129 Bologna, Italy
[7] Osservatorio Astronomico di Roma (INAF), via Frascati 33, 00040 Monteporzio Catone, Roma, Italy

Received 3 November 2008 / Accepted 11 March 2009

ABSTRACT

Context. This paper presents the X-ray properties of a flux- and volume-limited complete sample of 16 giga-hertz peaked spectrum (GPS) galaxies.
Aims. This study addresses three basic questions in our understanding of the nature and evolution of GPS sources: a) What is the physical origin of the X-ray emission in GPS galaxies? b) Which physical system is associated with the X-ray obscuration? c) What is the "endpoint" of the evolution of compact radio sources?
Methods. We discuss in this paper the results of the X-ray spectral analysis, and compare the X-ray properties of the sample sources with radio observables.
Results. We obtain a 100% (94%) detection fraction in the 0.5–2 keV (0.5–10 keV) energy band. GPS galaxy X-ray spectra are typically highly obscured ($\langle N_{\rm H}^{\rm GPS}\rangle = 3\times10^{22}$ cm^{-2}; $\sigma_{N_{\rm H}} \simeq 0.5$ dex). The X-ray column density is larger than the HI column density measured in the radio by a factor 10 to 100. GPS galaxies lie well on the extrapolation to high radio powers of the correlation between radio and X-ray luminosity known in low-luminosity FR I radio galaxies. On the other hand, GPS galaxies exhibit a comparable X-ray luminosity to FR II radio galaxies, notwithstanding their much larger radio luminosity.
Conclusions. The X-ray to radio luminosity ratio distribution in our sample is consistent with the bulk of the high-energy emission being produced by the accretion disk, as well as with dynamical models of GPS evolution where X-rays are produced by Compton upscattering of ambient photons. Further support to the former scenario comes from the location of GPS galaxies in the X-ray to O[III] luminosity ratio versus $N_{\rm H}$ plane. We propose that GPS galaxies are young radio sources, which would reach their full maturity as classical FR II radio galaxies. However, column densities $\gtrsim10^{22}$ cm^{-2} could lead to a significant underestimate of dynamical age determinations based on the hotspot recession velocity measurements.

Key words. galaxies: jets – galaxies: active – X-rays: galaxies

1. The nature of GPS radio galaxies

This paper presents an X-ray study of a complete radio-selected sample of Giga-Hertz Peaked Spectrum (GPS) galaxies. GPS sources are characterised by a simple convex radio spectrum peaking near 1 GHz (Stanghellini 2006; Lister 2003; O'Dea 1998). They represent about 10% of the 5-GHz selected sources. About half of known GPS sources are morphologically classified as galaxies, the remaining as quasars. They often exhibit symmetric, very compact (10–100 pc) structures, reminiscent of those present in extended radio galaxies on much larger scales.

Little is known about their high-energy emission. GPS galaxies are rather elusive in X-rays (O'Dea et al. 1996). X-ray spectroscopic studies prior to modern X-ray observatories were inconclusive on whether this low detection rate is due to intrinsic weakness or to obscuration of the active nucleus (Elvis et al. 1994a). Deep *Chandra* and XMM-Newton observations of GPS galaxies are scanty. One of the few exceptions is a deep XMM-Newton pointing of 3C 301.1 (O'Dea et al. 2006); it unveiled a hard X-ray emission component, which could be associated with hot gas shocked by the expansion of the radio source or to synchrotron self-Compton emission. Analysis of small samples of GPS galaxies observed with XMM-Newton were presented by Vink et al. (2005) and Guainazzi et al. (2006). Our paper represents an extension of their results.

Understanding the origin of high-energy emission in these objects may have important implications on the birth and evolution of the "radio power" in the Universe. GPS sources were originally suggested to represent radio galaxies in the early stage of their life (typical ages $<10^4$ years, Fanti et al. 1995; Murgia 2003). This possibility was recently supported by the detection of mas-hotspot proper motions (Poladitis & Conway 2003; Gugliucci et al. 2005). Alternatively, as originally suggested by Gopal-Krishna & Wiita (1991), GPS sources could remain compact during their whole radiative lifetime, because interaction with dense circumnuclear matter impedes their full growth.

In order to address the above issues, and provide the best possible estimate of the gas density in the GPS galaxy nuclear environment, we have undertaken an XMM-Newton observation program of a radio-selected complete sample of GPS galaxies. The three main issues which originally motivated our study, and will be discussed throughout the paper, are:

– What is the physical origin of the X-ray emission in GPS galaxies?

Table 1. The GPS sample discussed in this paper.

NED name	J2000 name	z^a	Observation ID^b	Observation date	Reference^c
4C+00.02	002225+001456	0.305	0407030101	2006-Jun.-26	(1)
COINSJ0111+3906	011137+390628	0.668	0202520101	2004-Jan.-09	(2)
PKS0428+20	043103+203734	0.219	0407030201	2006-Sep.-02	(1)
PKS0500+019	050321+020305	0.585	0205180601	2004-Aug.-18	(3)
B30710+439	071338+434917	0.518	0202520201	2004-Mar.-23	(2)
PKS0941−080	094336−081931	0.228	Chandra		(3)
B1031+567	103507+562847	0.450	0202520301	2004-Oct.-21	(2)
4C+14.41	112027+142054	0.362	0502510201	2007-Jun.-13	(1)
4C+32.44	132616+315409	0.370	0502510301	2007-Dec.-05	(1)
PKS1345+125	134733+121724	0.122	ASCA		(4)
4C+62.22	140028+621038	0.431	0202520401	2004-Apr.-14	(2)
OQ+208	140700+133438	0.077	0140960101	2003-Jan.-31	(5)
PKS1607+26	160913+264129	0.473	0502510401	2008-Jan.-17	(1)
			0502510801	2008-Jan.-19	
PKS2008−068	201114−064403	0.547	0502510501	2007-Oct.-12	(1)
PKS2127+04	213032+050217	0.990	0502510601	2007-May-17	(1, 6, 7)
COINSJ2355+4950	235509+495008	0.238	0202520501	2003-Dec.-26	(2)

[a] Data taken from NED.
[b] XMM-Newton observation ID.
[c] (1) This paper; (2) Vink et al. (2005); (3) Guainazzi et al. (2006); (4) O'Dea et al. (2000); (5) Guainazzi et al. (2004); (6) Siemiginowska et al. (2005); (7) Siemiginowska et al. (2008).

– Which physical system is associated with the X-ray obscuration?
– What is the "endpoint" of the evolution of compact radio sources?

This paper is structured as follows: in Sect. 2 we present the sample. The data reduction procedure and the results of the spectral analysis on the unpublished sources are presented in Sects. 3 and 4, respectively. This paper does not discuss the X-ray spectral analysis of sources published elsewhere (Guainazzi et al. 2006; Vink et al. 2005). In Sect. 5 we summarise the X-ray properties of the whole GPS sample, and compare these with a control sample of large-scale radio galaxies. Finally, we discuss our results in Sect. 6, and summarise our findings and their possible implications on the evolution of GPS sources in Sect. 7. We adopt throughout the paper a cosmology with $H_0 = 70$ km s^{-1} Mpc^{-1}, $\Omega_\Lambda = 0.73$, and $\Omega_m = 0.27$ (Spergel et al. 2007).

2. The sample

The sources discussed in this paper constitute a flux- and volume-limited sub-sample extracted from the complete radio-selected sample of GPS galaxies of Stanghellini et al. (1998). We'll refer to this sub-sample as "our GPS sample" hereafter. We selected all sources with redshift $z < 1$, and flux density at 5 GHz ≥1 Jy. The whole sample (16 sources) has been observed with XMM-Newton across different observing cycles. The only exceptions are PKS 0941–08 and PKS1345+125, for which archival *Chandra* and ASCA data are available, respectively. Preliminary results, based on a small sub-sample of 5 objects, were presented in Guainazzi et al. (2006)[1]. Some of the sample sources were included in Vink et al. (2005). The whole sample is listed in Table 1. A more general discussion of the X-ray and multiwavelength properties of our whole GPS sample is deferred to Sect. 5. A summary of the X-ray and radio properties of the whole sample is in Appendix B.

[1] Guainazzi et al. (2006) present also data of COINSJ0029+3456; this source was later discovered to host a blazar, and won't be considered in the sample discussed in this paper.

Table 2. Properties of the X-ray observations discussed in this paper. Exposure times (T_{exp}) and Count Rates (CR) refer to the pn in the 0.5–10 keV band (unless otherwise specified). τ is the count rate threshold applied in the determination of the Good Time Interval for scientific product extraction (details in text). ρ is the radius of the scientific products extraction region. $N_{H,Gal}$ is the column density due to gas in the Milky Way along the line-of-sight to the GPS galaxy (Kalberla et al. 2005) in units of 10^{20} cm^{-2}.

Source	$N_{H,Gal}$	T_{exp} (ks)	τ (s^{-1})	ρ ($''$)	CR (10^{-3} s^{-1})
4C+00.02	2.7	22.2	2.1	...	[a]
PKS0428+20	19.6	15.4	0.75	23	7.1 ± 0.8
4C+14.41	2.0	16.3	0.5	15	4.8 ± 0.8
4C+32.44	1.2	20.5	0.5	16	25.6 ± 1.2
PKS1607+26	3.8	18.5	18	20	39 ± 7
PKS2008−068	5.0	23.2	0.75	15	2.0 ± 0.4
PKS2127+04	5.0	10.8	0.5	25	21.2 ± 1.9

[a] Detected only in the soft X-ray band (0.5–2 keV), with a count rate: $(2.3 \pm 0.7) \times 10^{-3}$ s^{-1}.

3. Observations and data reduction

In this paper (as also originally done by Guainazzi et al. 2006; and Vink et al. 2005) we will consider only X-ray data taken with the XMM-Newton EPIC cameras (pn, Strüder et al. 2001; MOS, Turner et al. 2001), because the sources were too faint to yield a measurable signal in the high-resolution RGS cameras. Observational information for the sources for which new measurements are presented here is listed in Table 2.

XMM-Newton data were reduced with SASv7.1 (Gabriel et al. 2003) according to standard procedures as in, e.g., Guainazzi et al. (2006). The most updated calibration files available at the date of the analysis (February 2008) were used. Source scientific products were accumulated from circular regions surrounding the position of the optical nucleus of each source (extracted from the NED catalogue)[2]. The size of the source extraction regions are shown in Table 2. Following Guainazzi (2008), background scientific products were extracted

[2] `http://nedwww.ipac.caltech.edu/`

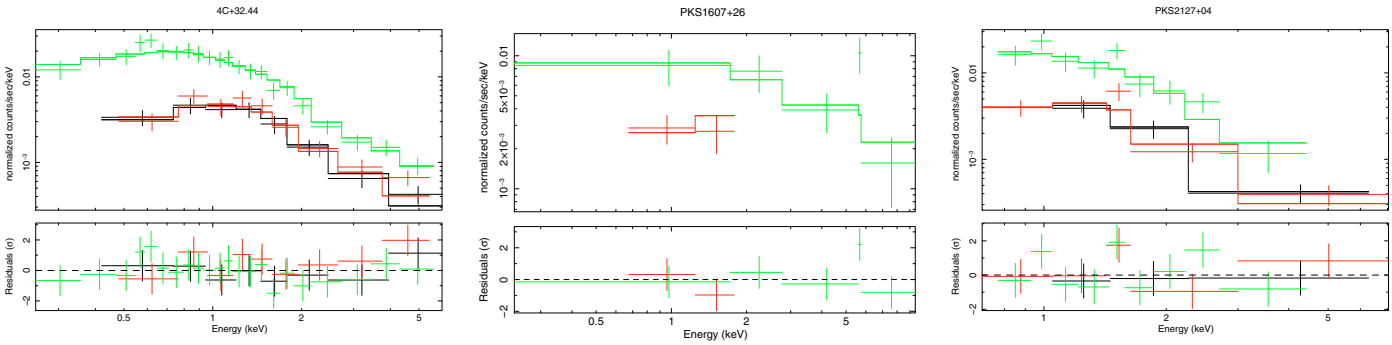

Fig. 1. Spectra of the three EPIC instruments (*upper panels*), and residuals in units of standard deviation (*lower panels*) when the baseline model is applied. In addition to the binning applied to the spectra to ensure the applicability of the χ^2 goodness-of-fit test, the spectra were further rebinned in this figure such that each spectral channel corresponds to a signal-to-noise ratio >3 for plotting purposes only. *Green*: pn; *black*: MOS 1; *red*: MOS 2.

Table 3. Best-fit parameters and results for the sources where spectral analysis was possible.

Source	$N_{\rm H}$ (10^{21} cm^2)	Γ	F_{2-10} (10^{-13} ergs cm^{-2} s^{-1})	$\log(L^a_{2-10})$	Fe K$_\alpha$ EW (keV)	χ^2/ν
4C+32.44	$1.2\pm^{0.6}_{0.5}$	1.74 ± 0.2	0.78 ± 0.13	$43.57\pm^{0.05}_{0.06}$	<1.0	20.6/36
PKS1607+26	<2	0.4 ± 0.3	$4.2\pm^{1.5}_{0.6}$	44.27 ± 0.01	<0.7	32.2/21
PKS2127+04	<19	$1.98^{+0.5}_{-0.4}$	$0.49\pm^{0.12}_{0.17}$	44.46 ± 0.06	<0.9	14.7/16

[a] In erg s^{-1}.

from source free circular regions close to the source and on the same CCD as the source for the MOS cameras; and from source-free regions centred at the same row in detector coordinates as the source in nearby CCDs for the pn. As many of the sources were X-ray faint, particular care has been applied in the choice of flaring particle background rejection thresholds optimising the signal-to-noise ratio of the final scientific products. Using a single-event, $E > 10$ keV full field-of-view light curve as a monitoring tool of the instantaneous intensity of the background, ten different logarithmically spaced thresholds between 0.1 s^{-1} and about two times the highest light curve count rates were tried. For each threshold the radius of the source extraction region was also varied to obtain the highest number of net counts for a given signal-to-noise ratio. Spectra were binned in such a way to avoid oversampling of the intrinsic instrumental energy resolution by a factor larger than 3, and to have at least 25 background-subtracted counts in each spectral bin. These conditions ensure the applicability of the χ^2 statistic as a goodness-of-fit test.

In this paper, errors on the spectral parameters and on any derived quantities are at the 90% confidence level for one interesting parameter; errors on the count rates and derived quantities are at 1σ level. Whenever statistical moments or correlations on distributions including upper limits are calculated, an extension of the regression method on censored data originally described by Schmitt (1985) and Isobe et al. (1986) has been used. More details on this method were presented by Guainazzi et al. (2006).

4. Results

In this Section we present spectral-analysis for the 7 unpublished sources in our GPS sample.

No significant variability in either integrated X-ray flux or spectral shape was detected in any source presented in this paper on timescales $\lesssim 10^4$ s. We therefore focus on the properties of their time-averaged spectra.

For 3 of these sources the number of degrees of freedom in the binned spectra was larger than 4: 4C+32.44, PKS1607+26, PKS 2127+04. In these cases a standard spectral analysis was possible. The spectra were fitted in the 0.2–10 keV energy range with Xspec (version 11; Arnaud 1996). A model consisting of three components was used:

$$e^{-N_{\rm H,Gal}\sigma(E)} \times e^{-N_{\rm H}\sigma[E(1+z)]} \times KE^{-\Gamma} \quad (1)$$

where the photo-electric absorption components use Wisconsin cross-sections (Morrison & McCammon 1983), and K is the unabsorbed spectral normalisation at 1 keV. We'll refer to this model as our "baseline" model hereafter. The column density $N_{\rm H,Gal}$ was kept fixed to the contribution by intervening gas in the Galaxy as measured in the Leiden/Argentine/Bonn (LAB) Survey of Galactic HI (Kalberla et al. 2005)[3], whereas $N_{\rm H}$ is the column density of local gas at the galaxy redshift. The results of the spectral fitting are shown in Fig. 1 and summarised in Table 3. X-ray luminosities in this table and hereafter are K-corrected and based on the best-fit model for each source. Addition of a Gaussian profile to the baseline model to characterise line emission never improved significantly the quality of the fit. The upper limits on the Equivalent Width (EW) of an unresolved Fe K$_\alpha$ neutral fluorescent line are also reported in Table 3. They are generally inconclusive. Best-fit models and residuals are shown in Fig. 1.

For 4 other sources (4C+00.02, PKS 0428+20, 4C+14.41, and PKS 2008−068) the low signal-to-noise did not allow for spectral analysis. We have therefore based our estimation of the spectral parameters of the baseline model on the Hardness Ratio

[3] `http://heasarc.gsfc.nasa.gov/cgi-bin/Tools/w3nh/w3nh.pl`

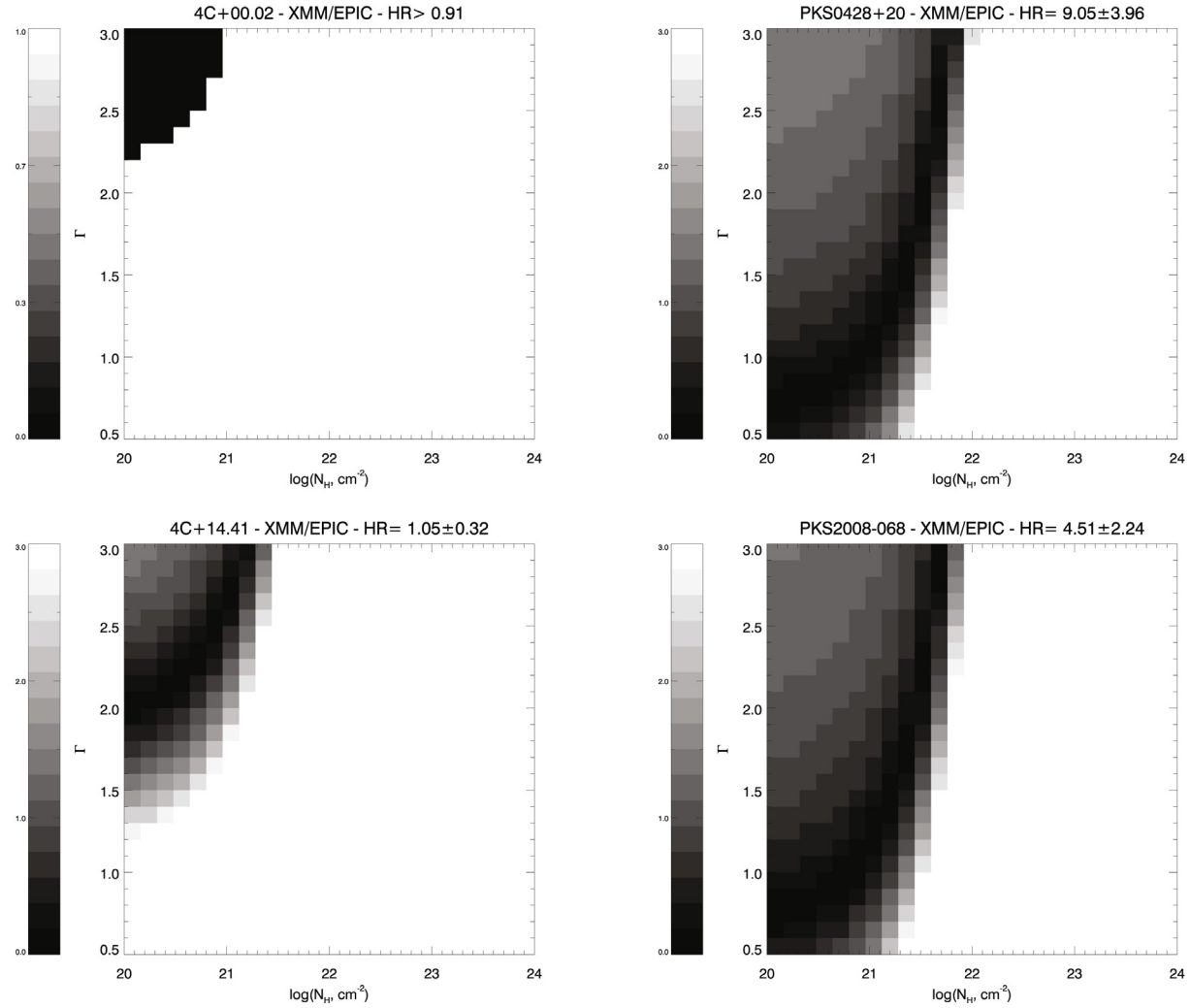

Fig. 2. Confidence level loci in the (Γ, $N_{\rm H}$)-plane. For 4C+00.02 the white area shows the locus of the parameter space where the model is consistent with the measured HR. In the other panels the grey scale indicates the deviation from the measured HR in units of standard deviations.

(HR), here defined as the ratio between the counts in the energy bands 1–10 keV and 0.2–1 keV. The measured HRs (or lower limit thereof) have been compared with the predictions of grids of simulated baseline models. Iso-HR contour plots in the Γ ([0.5:3]) versus $N_{\rm H}$ ([10^{20}, 10^{24} cm^{-2}]) parameter space were built (see Fig. 2) The confidence interval in column density was estimated as the minimum and maximum value of the 1.6σ interval around the curve corresponding to the nominal HR, when Γ was constrained in the range: [0.63, 2.62]. The photon-index range corresponds to the $\langle\Gamma\rangle \pm 3\sigma$ interval of the Γ distribution, calculated on the whole sample of GPS galaxy for which the data quality allowed us to perform a spectral analysis (cf. Fig. 6). The resulting constraints on the column density are shown in Table 4.

Table 4. Constraints on the intrinsic column density derived from iso-HR contours in the Γ versus $N_{\rm H}$ parameter space. No constraint can be derived for 4C+00.02.

Source	$N_{\rm H,max}$ (10^{21} cm^{-2})	$F_{2-10}{}^{a}$	$\log(L_{2-10})$
PKS0428+20	<6.9	[0.3, 0.6]	43.1
4C+14.41	<1.6	[0.2, 0.5]	43.1
PKS2008−068	<4.8	[0.2, 0.5]	43.8

[a] Ranges in units of 10^{-13} erg s^{-1} cm^{-2} corresponding to the $N_{\rm H}$ range as in this table, and to the photon index in the range: [0.63,2.62] (more details in text).

4.1. A Compton-thick AGN in PKS1607+26?

The fit of the EPIC spectra of PKS1607+26 yields an unusually flat spectral index: $\Gamma = 0.4 \pm 0.3$. A flat spectrum may be indicative of a blazar-type spectral component. Alternatively, in radio-quiet AGN spectral indices $\Gamma \simeq 0$ are generally interpreted as evidence for a Compton-thick AGN, whose primary X-ray emission is totally suppressed by optically thick matter with a column density $N_{\rm H} > \sigma_{\rm t}^{-1} \simeq 1.6 \times 10^{24}$ cm^{-2} (see Comastri 2004, for a review). In Compton-thick AGN, residual X-ray emission red-wards the photoelectric cutoff could be due to Compton-reflection of the otherwise invisible primary radiation off the obscuring matter[4]. Fe K$_\alpha$ fluorescent emission with large *EW* ($\gtrsim$600 eV, Risaliti 2002; Guainazzi et al. 2005) is the unmistakable "smoking gun" of a Compton-thick AGN. We have therefore applied the baseline spectral model for Compton-thick AGN to the PKS1627+06 pn spectrum (the MOS spectra have very poor statistics, and do not provide any further

[4] On an "historical" note, the GPS galaxy OQ+208 was the first radio-loud Compton-thick AGN ever discovered (Guainazzi et al. 2004).

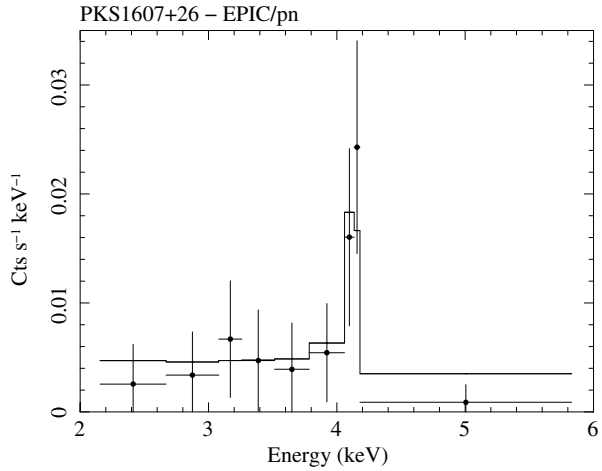

Fig. 3. EPIC-pn spectrum of PKS1607+26 in the 2–10 keV energy band (observer's frame). The data points have been rebinned such that each displayed spectral channel has a signal-to-noise ratio larger than 1. The *solid line* represents the best-fit reflection-dominated model (details in text).

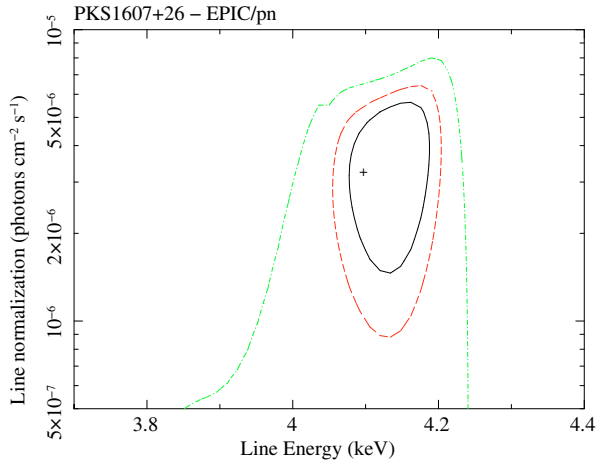

Fig. 4. Iso-χ^2 contours in the centroid energy (observer's frame) versus normalisation plane for the Gaussian profile in the best-fit reflection-dominated model for PKS1607+26. The contours correspond to the 68%, 90% and 99% confidence level for two interesting parameters, respectively.

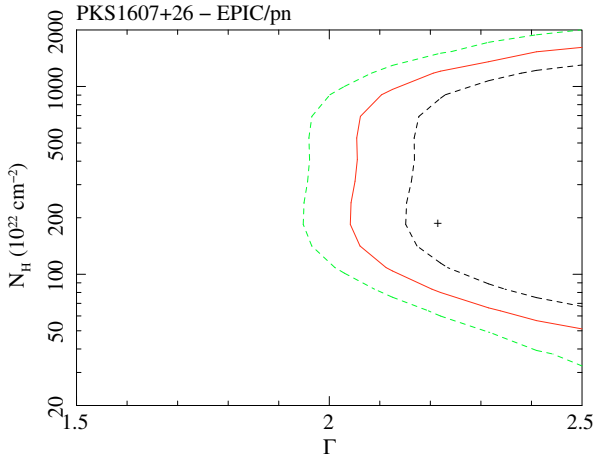

Fig. 5. Iso-χ^2 contours for the column density covering a power-law primary continuum derived from the EPIC pn spectrum of PKS1607+26 in the reflection-dominated scenario. The *lines* correspond to the 68%, 90% confidence level for one interesting parameter and to the 90% confidence level for two interesting parameters, respectively.

constraints): a pure Compton-reflection continuum (model `pexrav` in Xspec, Magdziarz & Zdziarski 1995) plus a Gaussian unresolved emission line. In order to take advantage of the full energy resolution of the EPIC cameras we fit the unbinned spectrum using the Cash statistic, C (Cash 1976). Although the Cash statistic does not provide an absolute level of statistical confidence on the quality of the fit, the resulting value (C = 25.2/21 degrees of freedom) and the smoothness of the residuals (Fig. 3) indicate that the fit is good. Once this continuum is adopted, an emission line is required at a confidence level larger than 90% for two interesting parameters (or 95% for one parameter; Fig. 4). The EW (500 ± 300 eV) is consistent with values typically observed in Compton-thick AGN. However, the best-fit centroid energy of this feature ($E_c^{z=0}$ = $4.12\pm^{0.06}_{0.05}$ keV) is slightly inconsistent with Fe K$_\alpha$ fluorescence if converted into the rest frame with the quoted redshift for this object: $E_c^{z=0.473}$ = $6.06\pm^{0.09}_{0.07}$ keV. No other known atomic transition could be responsible for a feature at this energy. We do not have a convincing explanation for this finding. The redshift quoted in the literature for PKS1607+26 dates back to Philips & Shaffer (1983). A couple of years later Biretta et al. (1985) refer to previous mis-identification of this object, and indeed the value of z = 0.47 in the original paper corresponds to the wrong identifier in Biretta et al. (1985). If the emission line is indeed the Fe K$_\alpha$, the redshift is $z \simeq 0.55$. Notwithstanding the ultimate redshift value, the very flat hard X-ray spectral index, alongside the detection of a strong emission-line feature point to a Compton-thick nature for this object. In order to determine a lower-limit to the column density covering the primary continuum, we have added to the pure reflection model a power law obscured by photoelectric absorption. We have used a combination of the models `phabs` and `cabs` in Xspec to take into account the contribution of Compton scattering, which is no longer negligible for column densities close to the Compton-thick limit. The obscuring column density is constrained to be larger than 6×10^{23} cm^{-2} (90% confidence level for one interesting parameter; Fig. 5). This is the value we'll associate with PKS1607+26 in all subsequents plots and distribution functions. However, given the pending uncertainties on the ultimate identification of this source, we won't use this measurement to derive statistical estimators in the N_H distribution of the whole sample.

5. Comparison with control samples of "normal" radio galaxies

In this section we present X-ray spectral properties of the flux density and redshift-selected complete sub-sample extracted from the Stanghellini et al. (1998) GPS sample described in Sect. 2. Readers are referred to the Guainazzi et al. (2006) and Vink et al. (2005) papers for the spectral analysis of the sources not discussed in this paper. We have repeated the analysis of the sources of the Vink et al. (2005) with the same reduction and data screening criteria as in the Guainazzi et al. (2006) and in this paper. The results of our re-analysis are consistent with theirs. 5 GHz luminosities are taken from Stanghellini et al. (1998) and O'Dea (1998).

Our goal is also to compare the properties of the complete radio-selected flux-limited GPS sample with a control sample

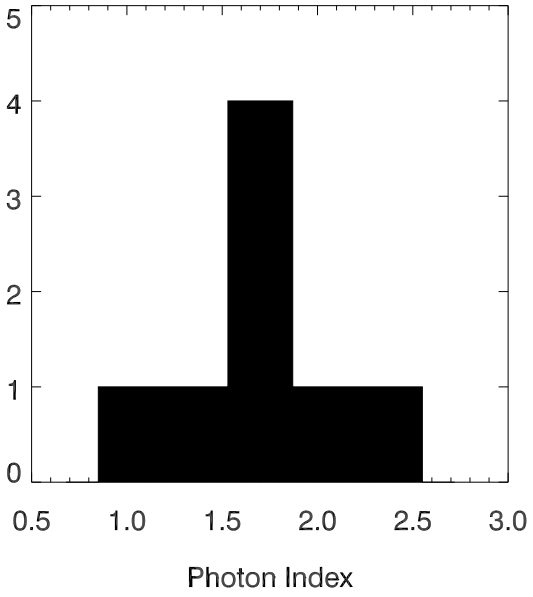

Fig. 6. Distribution of the photon index for the GPS sub-sample (8 objects), where data quality warranted spectral analysis.

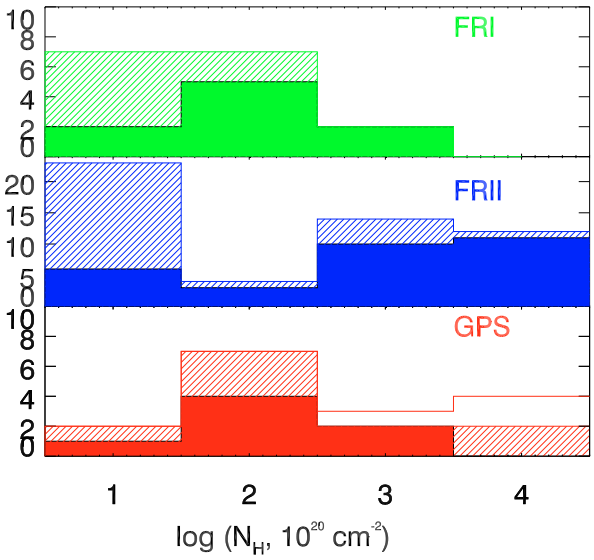

Fig. 7. Distribution of the core obscuring column densities for the GPS sample (*bottom panel*), the FR I (*upper panel*) and FR II (*middle panel*) control samples. *Shaded areas* indicate upper limits; *empty areas* indicate lower limits.

of "normal" radio galaxies. The control sample has been built from results recently published in the literature. It is based on observations of $z < 1$ radio galaxies taken by ASCA (Sambruna et al. 1999), BeppoSAX (Grandi et al. 2006), XMM-Newton and *Chandra* (FR I: Donato et al. 2004; Evans et al. 2006; Balmaverde et al. 2006, FR II: Belsole et al. 2006; Evans et al. 2006; Hardcastle et al. 2006). Only one measurement per source has been retained in the control sample, based on the latest published result. However, we have considered the latest *Chandra* measurement, even when a later XMM-Newton observation was available, under the assumption that the superior spatial resolution of the *Chandra* optics provides a more reliable measurement of the core emission. The control sample comprises 93 sources (32 FR I, 54 FR II, the remaining ones have no FR classification). We stress that the control sample is neither complete nor unbiased. Moreover, it is not well matched with our GPS sample in redshift. The probability that the redshift distribution of the GPS sample is the same as in the entire control sample is 2% only. This difference is mainly due to FR Is being generally at lower redshift than our GPS sample, whereas our GPS and the control FR II samples are well matched in redshift (cf. Fig. 8). Whenever pertinent, we will explicitly show in the following the redshift dependence of the observables, and discuss possible bias associated with comparing samples inhomogeneous in redshift coverage.

5.1. X-ray detection fraction

We obtain a very large detection fraction; all the sources of our sample yield a detection in the soft X-ray band (0.5–2 keV), whereas 15 out of 16 are detected in the full band (0.5–10 keV). All of them but one (PKS1345+125) were unknown in X-rays prior to our *Chandra* (see also Siemiginowska et al. 2008) and XMM-Newton observations.

5.2. Spectral shape

In Fig. 6 we show the distribution of spectral indices for the 8 GPS of our sample[5], where the number of counts is good enough for the spectral analysis to be possible. The distribution has a mean value $\langle\Gamma\rangle = 1.66 \pm 0.40$, and a standard deviation $\sigma_\Gamma = 0.36$. The weighted mean is $\Gamma = 1.61 \pm 0.05$ if the measurements are weighted according to the inverse square of their statistical uncertainties.

5.3. Obscuration

In Fig. 7 the distribution of column density for the GPS sources of our sample is shown. The mean value of the distribution is $\langle N_{\rm H}^{\rm GPS}\rangle = 3 \times 10^{22}$ cm^{-2} with a standard deviation $\sigma_{N_{\rm H}} \simeq 0.5$ dex. The same figure shows the comparison with the control sample. The core emission of FR I radio galaxies is generally unobscured or only mildly obscured. In the Donato et al. (2004) FR I sample, less than one-third of the sample exhibit excess obscuration above the Galactic contribution, with rest-frame column densities in the range 10^{20-21} cm^{-2}, thus significantly lower than observed in our sample. The average of the column density distribution in the FR I control sample is $\langle N_{\rm H}^{\rm FRI}\rangle = (3.3\pm^{2.1}_{0.7}) \times 10^{21}$ cm^{-2}.

FR II cores tend instead to include a heavily obscured component. However, a detailed quantitative comparison between the GPS and the FR II control sample is difficult. For 11 out of 54 FR II sources neither a measurement nor an upper limit on the column density is available in the literature. These sources are generally considered as unobscured (Hardcastle et al. 2006). Lack of inclusion of these sources could potentially bias the control sample $N_{\rm H}$ distribution towards higher values. Bearing this

[5] 4C+32.44, 4C+62.22, B03710+439, COINSJ2355+4950, PKS0500+019, PKS1345+125, PKS2127+04, OQ+208.

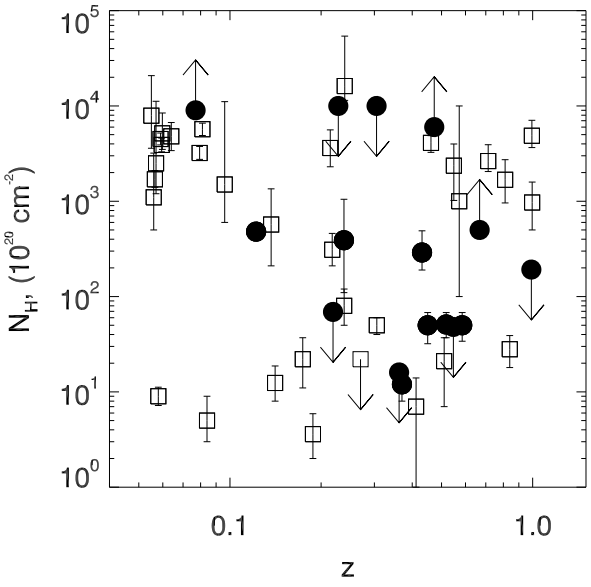

Fig. 8. Core obscuring column density as a function of redshift for the GPS galaxies (*filled dots*) and the FR II control sample (*empty squares*).

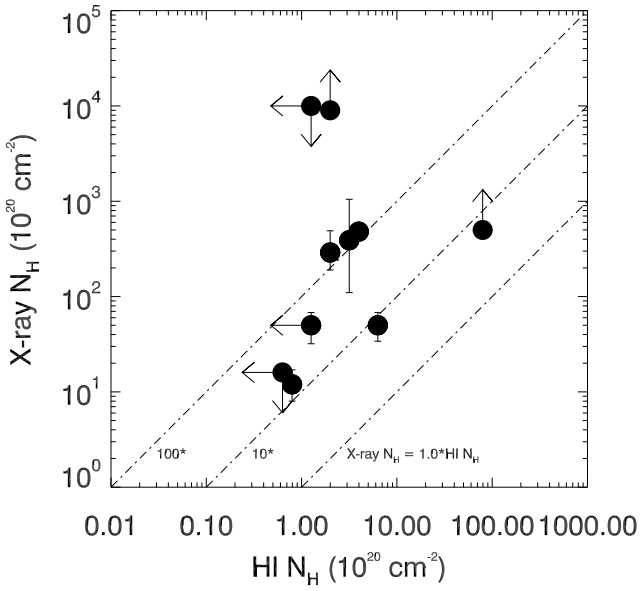

Fig. 9. Comparison between the column densities measured in X-rays (*this paper*) and with atomic hydrogen observations (Pihlström et al. 2003). The *lines* represent loci of constant X-ray versus HI column density ratio for ratio values of 1, 10, and 100 (from *right* to *left*), respectively.

caveat in mind, GPS galaxies seems to fill a gap in the N_H distribution between highly obscured ($\gtrsim 10^{23}$ cm^{-2}) and unobscured ($\lesssim 10^{22}$ cm^{-2}) FR II spectral components.

A potential area of concern is the comparison of column density measurements in samples, which are not well matched in redshift. However, Fig. 8 shows that this bias is not responsible for the difference between the average of the column density distribution in the GPS and FR II samples. Moreover, low-redshift GPS galaxies exhibit column densities not systematically lower than high-redshift ones.

Hardcastle et al. (2006) remark that heavily absorbed nuclei are rather common in narrow-line radio galaxies, whereas they are comparatively rare in Low-Excitation Radio Galaxies (LERG, Laing et al. 1994). There are 7 LERGs in our control sample; 5 of them have no column density measurement; the remaining two have column density of $\simeq 3 \times 10^{22}$ cm^{-2} (3C 123, Hardcastle et al. 2006) and $\simeq 10^{23}$ cm^{-2} (3C 427.1, Belsole et al. 2006). Taking into account the low number statistics and the uncertainties on the column density upper limits on formally "unobscured" LERGs, the comparison between X-ray obscuration in LERGs and GPSs is inconclusive.

The X-ray column density is significantly larger than the column density measured by HI observations by a factor 10 to 100. The comparison is shown in Fig. 9. The estimate of the HI column density depends on the values assumed for the spin temperature, T_s, and for the fraction of background source covered by the absorber, f_c. The data in Fig. 9 assume $T_s = 100$ K and $f_c = 1$ (Vermeulen et al. 2003; Pihlström et al. 2003; Gupta et al. 2006). The X-ray versus HI column density relation can be fit with a zero-offset linear function if T_s is of the order of a few thousands K (Ostorero et al. 2009). Alternatively, a low covering fraction could be responsible for the large X-ray to HI column density ratio, although this explanation is less likely given the large column densities measured in X-rays.

Holt et al. (2003) proposed an "onion-skin" model for the nuclear environment gas in B1345+125, to explain the

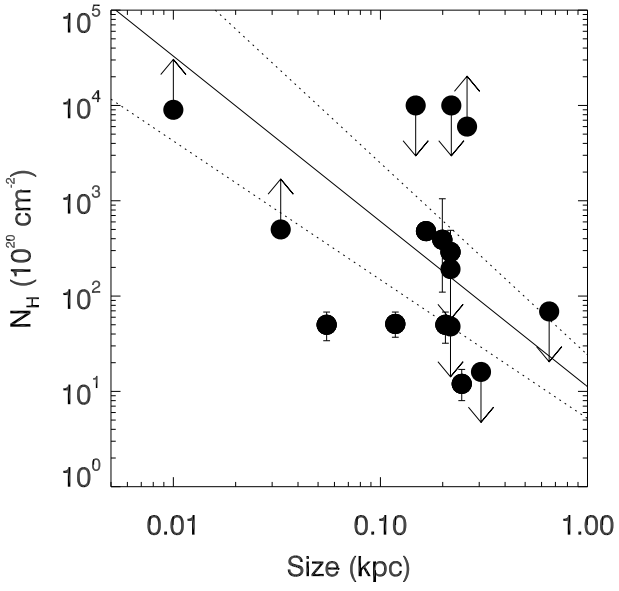

Fig. 10. X-ray column density versus the size of the radio structure. The *solid* line represent the best censored data linear fit with a function: $\log(N_H) = A + B \times \log(r_{kpc})$; the *dotted lines* correspond to $\pm 1\sigma$ uncertainties on the best-fit parameters.

reddening properties of the different components of the optical lines. The jet would pierce its way through a dense cocoon of gas and dust, with decreasing density at larger distances from the radio core. If this scenario would apply to the whole class of GPS samples, and X-ray and radio emission originate in the same

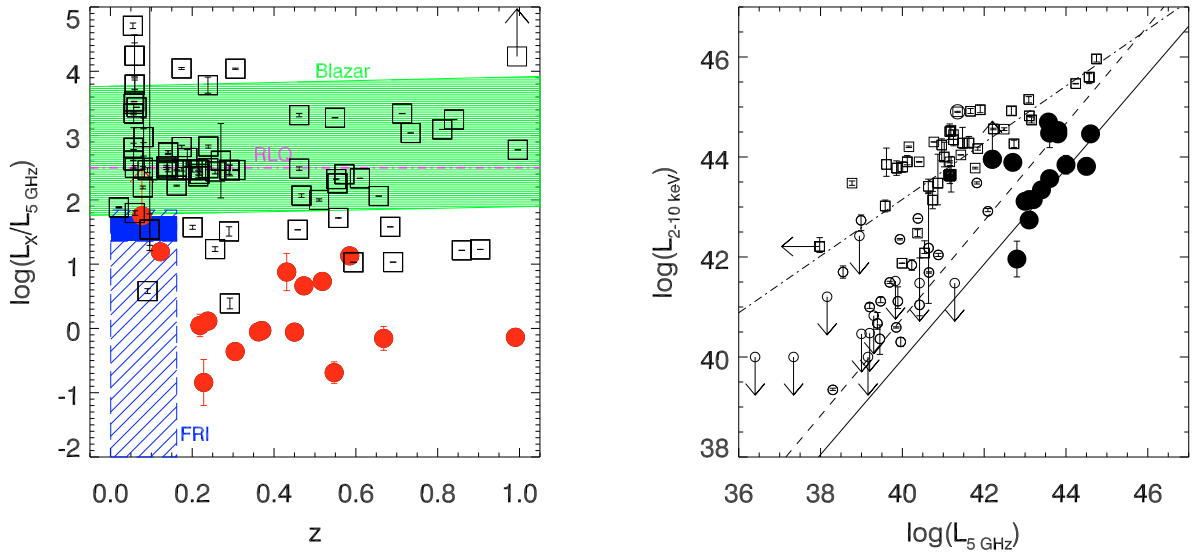

Fig. 11. *Left panel*: 2–10 keV versus 5 GHz logarithmic ratio versus redshift for the GPS (*filled dots*) and the FR II sample (*empty squares*). The *obliquely shaded box* indicates the locus of the FR I *Chandra* sample; the *horizontally shaded box* the locus of the blazar sample of Fossati et al. (1998); the *dot-dashed* line the locus corresponding to a typical Spectral Energy Distribution of a radio-loud quasar after Elvis et al. (1994b). *Right panel*: 2–10 keV versus 5 GHz core luminosity for the GPS galaxies (*filled circles*), and a control sample of radio galaxies (FR I:*empty circles*, FR II: *empty squares*). The *lines* represent the best-fit regression line for censored data for X-ray weak GPS (*continuous*), FR I (*dashed*) and FR II (*dashed-dotted*).

physical system, one might expect an anti-correlation between the measured column density and the size of the radio structure, with a large scatter due to the unknown line-of-sight angles distribution. This correlation is shown in Fig. 10. A censored fit on this data with a function: $\log(N_{\rm H}) = A + B \times \log(r_{\rm kpc})$ yields: $A = 21.4 \pm 0.4$, and $B = -1.2 \pm 0.3$, where $r_{\rm kpc}$ is the size of the radio structure in units of kpc. This result is formally robust, but admittedly mainly driven by the two extreme data points. A confirmation of this correlation by increasing the number of small ($r < 100$ pc) and large ($r > 1$ kpc) objects for which spectroscopic X-ray data are available is a task we are actively pursuing. Interestingly enough, an anti-correlation between the linear dimension of the sub-galactic radio galaxy and the radio HI column density was discovered by Pihilstöm et al. (2003). As already pointed out by Gupta et al. (2006), this anti-correlation could be driven by small sources probing gas closer to the AGN and hence at a higher spin temperatures. In this context, it is also interesting to observe that GPS *quasars* exhibit no absorption (with upper limits $\sim 10^{21}$ cm^{-2}; Siemiginowska et al. 2008), as well as diffuse emission associated with jets, binary structures or embedding clusters. The detection rate as well as the column density of HI absorption increases with core prominence (Gupta & Saikia 2006). The core prominence is a statistical indicator of the orientation of the jet axis to the line of sight. On the average HI absorbers are more common and exhibit larger column densities in galaxies than in quasars. This can be explained if the HI absorbing gas is distributed in a circumnuclear disk much smaller than the size of the radio emitting region, and only a small fraction of it is obscured in objects at large inclinations.

5.4. Radio-to-X-ray correlations

In the *left panel* of Fig. 11 we compare the logarithmic ratio between the 2–10 keV and the core 5 GHz luminosity ($L_{5\ \rm GHz} \equiv \nu_{5\ \rm GHz} \times S_{5\ \rm GHz}$, where $S_{5\ \rm GHz}$ is the luminosity density at 5 GHz) for the GPS and the control sample. Values for the GPS sample range between −0.5 and 1.5. No clear dependence on redshift is observed. GPS galaxies are X-ray under-luminous by about an order of magnitude with respect to their radio power once compared to FR II radio galaxies, blazars (Fossati et al. 1998) and radio-loud quasars (Elvis et al. 1994b). On the other hand, the X-ray-to-radio luminosity ratios in GPS galaxies well match values observed in FR I galaxies: $\log(L_{\rm X}/L_{5\ \rm GHz}) < 1.8$. It is important to stress again that there is almost no overlap in redshift between the GPS and the FR I samples, though.

The interpretation of X-ray-to-radio luminosity correlation depends on the origin of the bulk of the VLA radio emission in compact galaxies. VLBI observations of GPS galaxies unveiled a fraction of Compact Symmetric Objects (CSO) between ≃30% and 100% (Stanghellini et al. 1997, 1999; Xiang et al. 2005; Liu et al. 2007). Three objects in our sample exhibit a CSO morphology: PKS 0050+019, PKS 1345+125, and PKS 2008−068 (Stanghellini et al. 1997, 1999), although in all these cases the morphology is rather complex, with multiple component on scales $\lesssim$20 pc. High-resolution, multi-frequency observations of our sample would be required to ultimately estimate which fraction of the VLA flux can be safely attributed to a core.

From Fig. 11 a possible bimodality of the X-ray-to-radio luminosity ratio in the GPS sample is apparent. The fit of the cumulative distribution function of this quantity with a single Gaussian yields a Kolmogornov/Smirnov value of 0.33, corresponding to null hypothesis probability of about 4%. A fit with a double Gaussian yields instead a value of 0.18, with a null hypothesis probability of 65%. We consider this as a tentative piece of evidence for bimodality only. We will refer in the following to "X-ray bright" and to "X-ray weak" GPS galaxies as those, whose $\log(L_{\rm X})/(L_{5\ \rm GHz})$ ratio is larger/smaller than 0.5, respectively. No significant difference in the spectral shape between the

the "X-ray bright" and "X-ray weak" sources was observed. In particular, the obscuring column density distributions are indistinguishable.

In the *right panel* of Fig. 11 the 2–10 keV luminosity is plotted against the 5 GHz luminosity. In FR I galaxies a strong correlation between core X-ray, radio and optical flux is known (Chiaberge et al. 1999; Hardcastle & Worrall 2000). In our control sample, the slope of this correlation is consistent with unity: 0.97 ± 0.06. Interestingly enough, this slope is consistent with the slope observed in "X-ray weak" GPS galaxies 0.95 ± 0.12, with a $\simeq$0.5 dex offset at face-value. The "X-ray bright" sample exhibits a significantly flatter slope, although with large uncertainties (0.1 ± 0.2). Again, it is hard to estimate any bias associated with the coarse spatial resolution of the GPS radio measurements.

6. Discussion

In this section we will review the main X-ray observational properties of our whole GPS sample, trying to address the three issues which originally motivated our study:

- What is the physical origin of the X-ray emission in GPS galaxies?
- Which physical system is associated with the X-ray obscuration?
- What is the "endpoint" of the evolution of compact radio sources?

6.1. X-ray spectral support for an accretion-disk origin

The distribution of spectral indices in the GPS sample by itself does not provide any stringent constraints on the origin of X-ray emission in GPS galaxies. The mean value, $\langle\Gamma\rangle = 1.66$ ($\sigma_\Gamma = 0.36$), is consistent with spectral components associated with the jet in radio galaxies ($\Gamma = 1.88 \pm 0.02$), as well as with accretion ($\Gamma = 1.76 \pm 0.02$, Evans et al. 2006), although is nominally closer to the latter. A possible clue may come from the fact that the column density measured in X-rays is invariably larger by 1–2 orders of magnitudes than that measured in radio. This finding could be naturally explained by X-rays being produced in a smaller region than the radio. On the average, the radio morphology of compact radio sources strikingly resembles that of large-scale radio doubles, although on a scale which is entirely confined within the optical narrow-line emission regions. Radio emission traces therefore the radio hotspot and lobes. X-rays could be instead generated by the base of the jet, or by the accretion disk.

Support for the X-rays arising from a relatively compact region comes from the comparison with radio-quiet AGN. Once a similar baseline model is employed, Seyfert Galaxies have: $\langle\Gamma_{\rm Sy}\rangle = 1.64 \pm 0.05$ (Bianchi et al., submitted)[6]. GPS galaxy X-ray spectra lack the complexity that Seyferts typically exhibit. There is no strong evidence for a soft excess (with the only exception of OQ+208, Guainazzi et al. 2004), warm absorber, warm scattering or Fe K_α fluorescent emission (with, again, the notable exceptions of OQ+208 and, possibly PKS1607+26) in our sample. However, most of the GPS galaxy spectra collected so far with either XMM-Newton or *Chandra* do not possess the statistical quality that would be needed for these additional spectral features to be unambiguously detected.

[6] This is *not* the intrinsic spectral index, which can be significantly larger due to the hardening effect of ionised absorbers of disk/torus reflection.

The scatter in the X-ray to radio luminosity ratio, and its lack of dependency with source size and age (cf. also Fig. 13) may indicate a link between accretion disk and jet activity primarily driven by disk instabilities. 10–20% of GPS objects exhibit very extended radio (Baum et al. 1990; Stanghellini et al. 1990; Schoenmakers et al. 1999; Marecki et al. 2003) or X-ray (Siemiginowska et al. 2002, 2003) emission. These components have been interpreted as remnants of past enhanced activity. A similar behaviour on much shorter time scales is observed in Galactic Black Hole Candidates and micro-quasars, such as GRS 1915+105 (Belloni et al. 2000; Fender et al. 2004). Jet blobs are supposed to be fed by the evacuation of the innermost accretion disk regions. This mechanism yields alternating X-rays- (disk-dominated) and radio-bright (jet blob-dominated) phases. Models based on disk radiation pressure instabilities reproduce well the timescales of these transitions (Czerny et al., in preparation), although they don't make specific predictions on the evolution of the spectral energy distribution yet.

6.2. Dilution by X-rays from radio-emitting regions?

Most likely, the baseline model is indeed too simple. X-ray absorption could be "diluted" by X-rays coming from the high surface-brightness radio components, thus complicating the interpretation of the results derived by our simple baseline model. This scenario would also explain the (still tentative) anti-correlation between the X-ray column density and the size of the radio source (Fig. 10). In larger sources, a larger fraction of the X-ray emission associated with the radio hot-spots or lobes may be visible beyond the rim of the obscuring matter. Should this indeed be the case, we should, however, observe deviations from a simple power-law spectral shape. We indeed observe a soft excess in the radio-loud Compton-thick GPS galaxy OQ+208. This is the closest object in our sample, and the only one where high-resolution spatially-resolved spectroscopy with *Chandra* could provide direct observational clues on the physical location of the X-ray emitting plasma.

6.3. The X-ray obscuring environment

Lacking other direct pieces of evidence from X-rays alone, one may use multiwavelength diagnostics to obtain further clues on the origin of the X-ray emission in GPS galaxies. A well established diagnostic tool for X-ray obscuration in radio-quiet AGN involves the comparison between the column density measured in X-rays the absorption-corrected ratio of X-ray to O[III] fluxes (Maiolino et al. 1998). In the context of Seyfert galaxies, this diagram is used to calibrate the latter quantity as an estimator for obscuration. We use here the same plot with a different purpose, namely to test whether the ionising continuum powering the Narrow Line Regions in GPS galaxies has the same properties as in Seyfert galaxies once normalised to the X-ray primary emission. If this is the case, one may conclude that the "normalising primary continua" share the same properties in the two populations. The results of this comparison are shown in Fig. 12. 5 objects in our GPS sample have spectroscopic O[III] measurements (O'Dea 1998; Labiano et al. 2005, 2008, and references therein). The "control sample" is a collection of Seyfert 2-galaxies measurements in Guainazzi et al. (2005). The agreement is good. Although more GPS data would be required to ensure a homogeneous coverage of this plane, this piece of evidence further points towards an accretion origin for the X-ray emission in GPS galaxies.

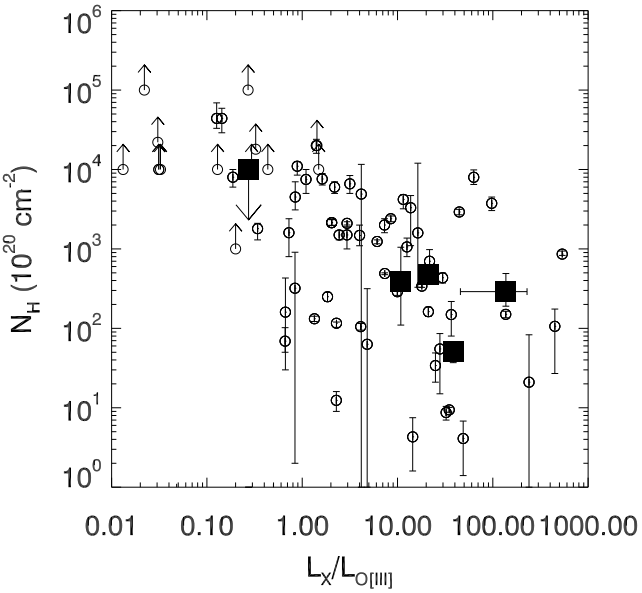

Fig. 12. X-ray column density versus the ratio between the absorption-corrected 2–10 keV and the O[III] fluxes. The *filled squares* are the 5 GPS galaxies in our sample for which O[III] measurements are available; the *empty circles* represent a sample of Seyfert 2 galaxies after Guainazzi et al. (2005).

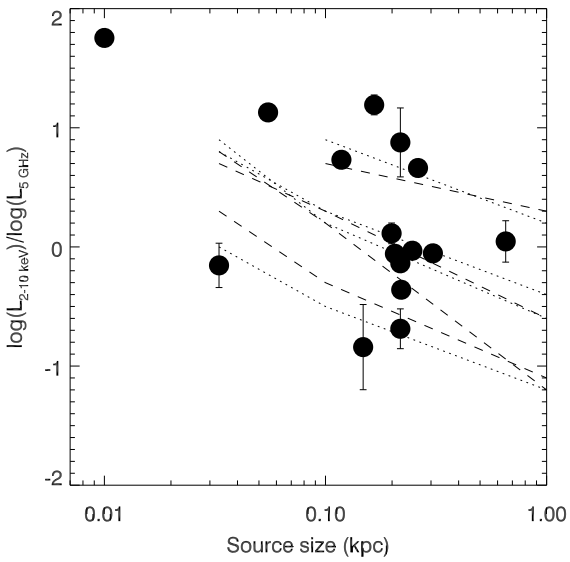

Fig. 13. X-ray to radio luminosity ratio versus the linear size for the sources of our GPS sample. The *lines* indicate the predictions of the Stawarz et al. (2008) model for jet kinetic powers ranging from 10^{44} erg s^{-1} to 10^{47} erg s^{-1}. *Dashed lines*: power-law injection function (Fig. 2 in their paper); *dotted lines*: broken power-law injection function (Fig. 3 in their paper).

Interestingly, the fraction of Compton-thick AGN in the GPS sample (0.12 ± 0.09, if PKS1607+26 is considered) is comparable to fractions observed in radio-quiet AGN (Heckman et al. 2005). Conversely, only one Compton-thick AGN has been detected in large-scale radio galaxies (Erlund et al. 2008), although FR II exhibit typically spectral components with very large obscuration (Belsole et al. 2006; Evans et al. 2006).

6.4. X-ray emission entirely associated with radio-emitting regions?

We now investigate the implications of the difference between X-ray and radio HI column densities, possibly due to the ionisation state of a single gas system covering simultaneously the radio and the X-ray emission. Attributing this difference solely to ionisation effects would mean ionisation fractions of 90% to 99% (see the discussion in Vink et al. 2005). Photoionisation simulations with CLOUDY (Ferland et al. 1998) show that this corresponds to an ionisation parameter $\gtrsim$20 for a gaseous nebula photoionised by a typical AGN continuum. An anti-correlation between the HI column density and the linear projected size of the radio source is now well established (Vermeulen et al. 2003; Pihlström et al. 2003; Gupta & Saikia 2006). Smaller sources (<0.5 kpc) tend to have larger HI column density than larger sources (>0.5 kpc). If not driven by uncertainties in the spin temperature of the HI absorbing gas, this anticorrelation can be explained by GPS galaxies hosting young radio sources, which evolve in a disk distribution of gas with a power-law radial density dependence. The same explanation could lay behind the (tentative) anti-correlation between X-ray column density and radio size in GPS galaxies (Fig. 10). One can assume a scenario where the radio and X-ray source are seen through the same line-of-sight and are both embedded in a screen of ionised gas, responsible for X-ray photoelectric absorption as well as for radio free-free absorption. From the definition of ionisation parameter, it follows for the X-ray regime:

$$n_{\mathrm{e},3} \gtrsim 10^2 R_{\mathrm{kpc}}^{-2} L_{44}$$

where $n_{\mathrm{e},3}$ is the plasma density in units of 10^3 cm^{-3}, R_{kpc} is the distance between the ionising source and the innermost side of the absorbing material in kpc, and L_{44} is the ionising luminosity in units of 10^{44} erg s^{-1}. It is plausible that densities in GPS sources are large enough that free-free absorption may play a role (O'Dea et al. 1991; Stawarz et al. 2008). The emission measure for free-free absorption at 5 GHz is (see, e.g., Osterbrock 1977):

$$n_{\mathrm{e}}^2 d_{\mathrm{pc}} \simeq 90 \tau T_4^{1.35}$$

where d_{pc} is the path length in parsecs and T_4 is the temperature in units of 10^4 K. Assuming $R \sim d$, one can constrain the plasma temperature:

$$T_4 \gtrsim (L_{44}\eta_{30})^{1.5} R_{\mathrm{kpc}}^{-2.2}$$

where η_{30} is the conversion factor between the absorption-corrected 2–10 keV and the bolometric luminosity in units of 30. For standard values of η_{30} (Elvis et al. 1994b), almost all GPS sources in our sample require temperature above that at the dust sublimation radius in this scenario. This outcome could be tested by measurements of the optical reddening in our sample.

If the compact jet "drills" its way through such a medium, would it be significantly decelerated or even "frustrated", i.e. permanently confined? This issue was discussed by Guainazzi et al. (2004) for the case of the Compton-thick absorber in OQ+208. They concluded that for large inclination angles or

large thickness of the Compton-thick layer, the jet could have been significantly decelerated by the interaction with the ambient medium. Although permanent confinement is unlikely in OQ+208, underestimating the evolution time scale by one-two orders of magnitude is possible. Let's revise their argument for the whole sample of GPS galaxy. The expansion time for a jet propagating under pressure equilibrium through an homogeneous medium can be expressed as (Scheuer 1974; Carvalho 1985, 1998):

$$t_{\rm e} \sim 6\ r_{100\ {\rm pc}}^{1.5} L_{\rm inj,44}^{-0.5} (\cos\iota)^{-1.5} \Omega_{10}^{0.5} N_{\rm H}^{0.5}\ {\rm s}$$

where $L_{\rm inj,44}$ is the (unknown) luminosity injected in the jet in units of 10^{44} erg s^{-1}, and Ω_{10} is the jet opening angle in units of 10 degrees. If we assume the censored best-fit for the linear size versus X-ray column density relation:

$$t_{\rm e} \sim 4 \times 10^5\ r_{100\ {\rm pc}}^{0.9} L_{\rm inj,44}^{-0.5} \Theta\ {\rm years}$$

where we have compacted all the geometrical factors in the variable $\Theta \equiv (\cos\iota)^{-1.5}\Omega_{10}^{0.5}$. There are admittedly several uncertainties in deriving the above scaling law. Most importantly, we know very little of the actual gas distribution in the environment surrounding compact radio sources (as well as in any other type of AGN). Still, the above estimate indicates that a GPS may expand during a time of the order of at least 10^5 years. This is longer then currently existing observational estimates (Poladitis & Conway 2003; Gugliucci et al. 2005), but not enough to make the hypothesis of permanent confinement viable.

6.5. Evolution of GPS sources

If the jet can indeed survive its eventful youth, and grow to reach a full level of kpc-scale maturity and beyond, what would it look like? The radio-to-X-ray luminosity plane does not ultimately elucidate the possible connection between GPS and "mature" radio galaxies. GPS galaxies are intriguingly well aligned along the extrapolation at high radio power of the correlation between radio core and X-ray luminosity valid for FR I radio galaxies (Evans et al. 2006). This correlation was proposed as a piece of evidence supporting a jet origin of unabsorbed X-ray spectral components in FR I radio galaxies. On the other hand, GPS galaxies have a comparable X-ray luminosity to FR IIs (cf. Fig. 11). In FR IIs, the obscured X-ray spectral component is probably associated with accretion onto the supermassive black hole obscured by a "torus", in analogy to the accepted paradigm applicable to radio-quiet AGN (Piconcelli et al. 2008). If the X-ray emission in GPS galaxies is due to accretion, the evolution of the radio and X-ray wavebands could be totally decoupled. Radio power would decline with the linear size (see, e.g., Fanti et al. 1995) while the sources expand through the ISM; at the same time the accretion disk would maintain a stable flow. At the end of their infancy, GPS galaxies would reach their glamorous maturity as FR II radio galaxies.

Evolutionary scenarios require that the radio luminosity of GPS sources decreases with evolution, not to exceed the number of observed FR II galaxies (Readhead et al. 1996). Recently, Stawarz et al. (2008) have proposed an evolutionary model for GPS sources, which explicitly predicts the dependency of the broadband Spectral Energy Distribution on the source linear size. In their model high-energy emission is produced by upscattering of various photon fields by the lobes' electrons. They predict a decrease of the X-ray to radio luminosity ratio by 1–2 orders of magnitude when the GPS source size increases from 30 pc to 1 kpc. In Fig. 13 we compare this prediction with our observations. There is no evidence for a strong anti-correlation between the two quantities; the slope of the best linear fit is 0.3±1.5 (1-σ statistical error). Still, the observational data are consistent with the Stawarz et al. model predictions, if the GPS galaxies in our sample cover a wide range in jet kinetic power.

It is still impossible with the available data to decide between an evolutionary scenario in which the source evolves into a conventional FR II or FR I radio galaxy. To achieve this goal, photometric X-ray observations of sizable samples of low-luminosity ($L_{5\ {\rm GHz}} \simeq 10^{40-42}$ erg s^{-1}) GPS galaxies would be crucial. Fortunately, it is now in principle possible to perform this experiment, thanks to the point-like source sensitivity and scheduling flexibility of *Chandra*.

7. Summary and conclusions

The main scope of this paper is reporting our current knowledge on X-ray emission in GPS galaxies. For the first time a complete radio-selected sample of GPS galaxies has been almost entirely observed with a modern X-ray observatory (mostly with XMM-Newton). The sample comprises all the $z < 1$ sources of the Stanghellini et al. (1998) sample having a 5 GHz flux density ≥1 Jy. The main results of our study can be summarised as follows:

- We obtain a very large detection fraction; all the sources of our sample yield a detection in the soft X-ray band (0.5–2 keV), whereas 15 out of 16 are detected in the full band (0.5–10 keV).
- In almost all cases, a simple power law modified by photoelectric absorption represents an adequate description of the 0.5–10 keV spectrum. In a few objects the number of net counts is not good enough to allow a full spectral analysis. In this case basic spectral parameters were derived from hardness ratios assuming the baseline model above.
- The mean of the spectral indices distribution is $\langle\Gamma\rangle = 1.66$ ($\sigma_\Gamma = 0.36$). Although the uncertainty on this parameter is still too large to pinpoint the physical mechanism responsible for the observed X-ray emission, at face value the Γ distribution is closer to those AGN classes, whose X-ray emission is believed to be dominated by accretion: Seyfert Galaxies and the obscured spectral component in FR II radio galaxies.
- We report the possible discovery of a Compton-thick AGN in PKS1607+26. Radio-loud Compton-thick AGN are still an elusive population (Comastri 2004). Together with OQ+208 – the other Compton-thick AGN in the sample – PKS1607+26 is the only GPS galaxy where an X-ray emission line has been detected, possibly associated with Fe K$_\alpha$ fluorescence.
- X-ray spectra of GPS galaxies are significantly obscured. The mean value of the column density distribution (without PKS1607+26, due to pending uncertainties on the identification of this source) is $\langle N_{\rm H}^{\rm GPS}\rangle = 3 \times 10^{22}$ cm^{-2} with a standard deviation $\sigma_{N_{\rm H}} \simeq 0.5$ dex. Such a value is much larger than column densities measured in a control sample of FR I radio galaxies, but still less than column densities covering accretion-related X-ray spectral components in FR II radio galaxies (Balmaverde et al. 2006; Belsole et al. 2006; Evans et al. 2006).
- The X-ray column density measured in almost all GPS galaxies is larger than the HI column density measured in the radio by a factor 10 to 100. This could be the signature of physically different absorption systems (Vink et al. 2005;

Guainazzi et al. 2006) or of a single system characterised by a spin temperature $\gtrsim 10^3$ K (Ostorero et al. 2009). We report a possible anti-correlation between the projected linear size of the radio source and the X-ray column density, analogous to the anti-correlation between radio size and HI column density reported by Pihlström et al. (2003) and Gupta et al. (2006).
- GPS galaxies occupy a specific locus in the radio versus X-ray luminosity plane. They lie well on the extrapolation to high radio powers of the correlation between these two quantities discovered in low-luminosity FR I radio galaxies. On the other hand, GPS galaxies exhibit a comparable X-ray luminosity to FR II radio galaxies, notwithstanding their much larger radio luminosity.
- GPS galaxies occupy the same locus as Seyfert galaxies in the O[III] to X-ray luminosity ratio versus X-ray column density diagnostic plane.

If the bulk of the X-ray emission in GPS galaxies is due to the accretion disk, one may expect that the X-ray and the radio source evolution in GPS galaxy would be decoupled. The accretion disk would maintain a stable flow of gas and (mostly sublimated) dust to the supermassive black hole, while the radio source fades away with its expansion into the ISM. This would imply an *increase* of the X-rays to radio luminosity ratio with size. On the other hand, models of the dynamical evolution of GPS sources, where the X-ray emission is primarily produced by Compton upscattering of ambient photons (Stawarz et al. 2008) predict a *decrease* of the X-ray to radio luminosity ratio with size. The $L_X/L_{5\ \mathrm{GHz}}$ ratios observed in our sample are consistent with both possibilities. Measurements in the γ-rays by *Fermi* (as originally proposed by Stawarz et al. 2008) could be crucial to discriminate between them. Alternatively, the large scatter observed in this quantity may be indicative of a coupling between the accretion disk and the jet activity driven by disk instabilities.

The evolutionary scenarios described above postulate that GPS sources are young objects, as also indicated by the direct measurement of their dynamical age. Eventually GPS galaxies would reach their full maturity as classical FR II radio galaxies. However, column densities $\gtrsim 10^{22}$ cm^{-2} fully surrounding the expanding radio source could significantly brake, if not entirely inhibit, this glazing future, leading to a significant underestimate of dynamical ages based on hotspots recession velocity measurements. Extending the number of X-ray measurements of low-luminosity ($L_{5\ \mathrm{GHz}} = 10^{40-42}$ erg s^{-1}) GPS galaxies is the next step we intend to pursue, in order to pinpoint the endpoint of their evolution.

Appendix A: a serendipitous blazar in the field of 4C+00.02

A bright off-axis sources is visible in the EPIC field of view of the XMM-*Newton* 4C+00.02 observation. This source will be referred in the following as XMMU J002200.8+000655. It is outside the field of view of the XMM-Newton Optical Monitor. The best-fit parameters when the baseline model is applied to its spectrum are summarised in Table A.1. The EW of a unresolved Fe K_α neutral fluorescent line is constrained to be lower than 400 eV.

This source was already known as 1RXS J002200.9+000659 (Voges et al. 1999). We have searched with Aladin for available measurements at other wavelengths. We have found data in GALEX GR4, SDSS (Adelman-McCarthy et al. 2008), 2MASS, and FIRST (White et al. 1997). In Fig. A.1 we compare the Spectral Energy Distribution (SED), with the average SED for radio-quiet and radio-loud quasars normalised at 1 keV (Elvis et al. 1994b) and with the "blazar track" corresponding to objects with the same radio luminosity as XMMU J002200.8+000655 (Fossati et al. 1998). As can be seen in Fig. A.1 the blazar SED track qualitatively agrees with the XMMU J002200.8+000655 SED. This source appears in NED as a BL Lac candidate, and in Véron-Cetty & Veron (2006) as a confirmed BL Lac object. Its optical spectrum was previously studied by Collinge et al. (2005), but heavy contamination by the host galaxy prevented its properties from being properly studied.

Table A.1. Fitting results for XMMU J002200.8+000655.

$N_H{}^a$ (10^{20} cm^{-2})	Γ	N (10^{-4} cm^{-2} s^{-1})	χ^2_ν/ν
$4.7^{+1.5}_{-1.6}$	$2.29^{+0.05}_{-0.06}$	7.40 ± 0.04	1.00/350

[a] In excess of the Galactic contribution along the line-of-sight to XMMU J002200.8+000655.

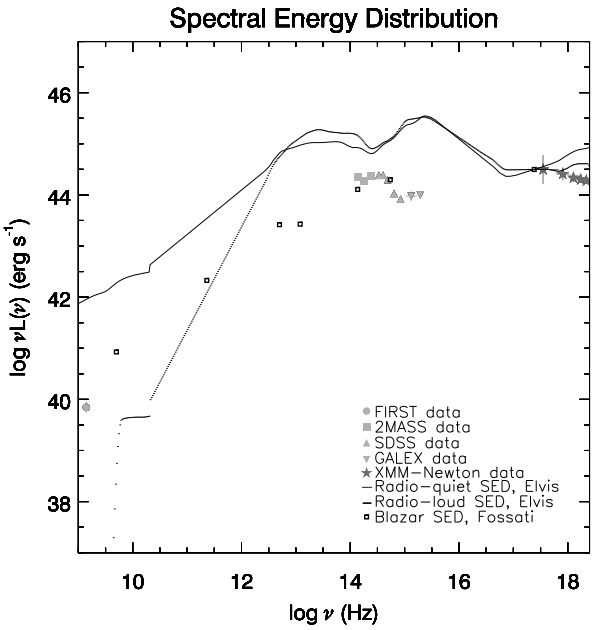

Fig. A.1. The Spectral Energy Distribution (SED) for XMMU J002200.8+000655. The photometric points are compared with standard SED for Blazars (boxes, Fossati et al. 1998) and radio-quiet and radio-loud quasars (dotted line and solid line, respectively; Elvis et al. 1994a), normalised at the value of XMMU J002200.8+000655 at 1 keV.

Appendix B: Summary of the radio and X-ray properties of the whole GPS sample

In Table B.1 we report a summary of the X-ray properties of the whole GPS sample discussed in this paper, together with the 5 GHz luminosity after O'Dea (1998) and Stanghellini et al. (1998).

Table B.1. X-ray properties and radio luminosity of the whole GPS sample discussed in this paper (Sects. 5 and 6).

Source name	$\log(L_{5\ \mathrm{GHz}}, \mathrm{erg\ s^{-1}})$	$L_{2-10\ \mathrm{keV}}$ (10^{43} erg s^{-1})	N_H (10^{20} cm^{-2})	Size (kpc)	HI $\log(N_\mathrm{H}, \mathrm{cm^{-2}})$	Γ
4C+00.02	43.1	0.55†	<10000	0.220	...	...
COINSJ0111+3906	44.0	7 ± 3	>500	0.033	21.9	...
PKS0428+20	43.1	1.4 ± 0.6	<70	0.653	20.5	...
PKS0500+019	43.6	50 ± 6	$50\pm^{18}_{16}$	0.055	20.8	$1.61\pm^{0.16}_{0.15}$
B30710+439	43.8	34.0 ± 0.2	$51\pm^{17}_{14}$	0.118	...	1.59 ± 0.06
PKS0941−080	42.8	0.091 ± 0.075	<10000	0.148	<20.1	...
B1031+567	43.4	2.2 ± 0.2	50 ± 18	0.206	<20.1	...
4C+14.41	43.2	1.40 ± 0.19	<16	0.306	<19.8	...
4C+32.44	43.6	3.7 ± 0.4	$12\pm^{6}_{5}$	0.247	19.9	1.7 ± 0.2
PKS1345+125	42.7	7.8 ± 1.5	480 ± 40	0.166	20.6	$1.1\pm^{0.7}_{0.8}$
4C+62.22	43.6	30 ± 20	$290\pm^{200}_{100}$	0.218	20.3	1.24 ± 0.17
OQ+208	42.2	>9.0	>9000	0.010	20.3	$2.21\pm^{0.19}_{0.14}$
PKS1607+26	43.8	29.0 ± 0.1	>6000	0.262	...	...
PKS2008-068	44.5	6 ± 2	<50	0.218	...	...
PKS2127+04	44.6	29 ± 4	<19	0.218	...	$2.0\pm^{0.5}_{0.4}$
COINSJ2355+4950	43.0	1.3 ± 0.3	$400\pm^{700}_{300}$	0.199	20.5	$1.8\pm^{1.6}_{0.9}$

† Extrapolated from the detection in the 0.5–2 keV band with $\Gamma = 1.61$ and $N_\mathrm{H} = N_{\mathrm{H,Gal}}$.

Acknowledgements. Based on observations obtained with XMM-Newton, an ESA science mission with instruments and contributions directly funded by ESA Member States and NASA This research has made use of data obtained through the High Energy Astrophysics Science Archive Research Centre Online Service, provided by the NASA/Goddard Space Flight Centre and of the NASA/IPAC Extragalactic Database (NED) which is operated by the Jet Propulsion Laboratory, California Institute of Technology, under contract with the National Aeronautics and Space Administration. O.T. thanks the whole ESA administration, and in particular Nienke de Boer, Marcus Kirsch and Fernando Maura, for their support during a six-month traineeship at ESAC, where most of the data analysis included in this paper was performed. This research is funded in part by NASA grant NNX07AQ55G. O.T. gratefully acknowledge an ESA Internal Fellowship Trainee grant. A.S. is partly supported by NASA contract NAS8-39073. The authors thank C. Stanghellini for a critical revision of an early version of this manuscript. Last, but not least, the authors gratefully acknowledge a careful and accurate referee report by Dr. D. J. Saikia, which greatly improved the overall presentation of the paper, while allowing us to better clarify some aspects of the radio measurements discussed in this paper.

References

Adelman-McCarthy, J. K., Agüeros, M. A, Allam, S. S., et al. 2008, ApJS, 175, 297
Arnaud, K. A. 1996, Astronomical Data Analysis Software and Systems V, ed. G. Jacoby, J., & Barnes, ASP Conf. Ser., 101, 17
Balmaverde, B., Capetti, A., & Grandi, P. 2006, A&A, 451, 35
Baum, S. A., O'Dea, C. P., de Bruyn, A. G., & Murphy, D. W. 1990, A&A, 232, 19
Belloni, T., Migliari, S., & Fender, R. P. 2000, 358, L29
Belsole, E., Worrall, D. M., & Hardcastle, M. J. 2006, MNRAS, 366, 339
Biretta, J. A., Schneider, D. P., & Gunn, J. E. 1985, AJ, 90, 2508
Carvalho, J. C. 1985, A&A, 150, 129
Carvalho, J. C. 1998, A&A, 329, 845
Cash, W. 1976, A&A, 52, 307
Chiaberge, M., Capetti, A., & Celotti, A. 1999, A&A, 349, 77
Collinge, M.-J., Strauss, M.-A., Hall, P.-B., et al. 2005, AJ, 129, 2542
Comastri, A. 2004, ASSL, 308, 245
Donato, D., Sambruna, R. M., & Gliozzi, M. 2004, ApJ, 617, 915
Elvis, M., Fiore, F., Wilkes, B., McDowell, J., & Bechtold, J. 1994a, ApJ, 422, 60
Elvis, M., Wilkes, B. J., McDowell, J. C., et al. 1994b, ApJS, 95, 1
Erlund, M. C., Fabian, A. C., Blundell, K. M., & Crawford, C. S. 2008, MNRAS, 385, L125
Evans, D. A., Worrall, D. M., Hardcastle, M. J., Kraft, R. P., & Birkinshaw, M. 2006, ApJ, 642, 96
Fanti, C., Fanti, R., Dallacasa, D., et al. 1995, A&A, 302, 317
Fender, R. P., Belloni, T. M., & Gallo, E. 2004, MNRAS, 355, 1105
Ferland, G. J., Korista, K. T., Verner, D. A., et al. 1998, PASP, 110, 761
Fossati, G., Maraschi, L., Celotti, A., Comastri, A., & Ghisellini, G. 1998, MNRAS, 299, 433
Gabriel, C., Denby, M., Fyfe, D. J., Hoar, J., & Ibarra, A. 2003, in Astronomical Data Analysis Software and Systems XIII, ed. F. Ochsenbein, M. Allen, & D. Egret (San Francisco: ASP), ASP Conf. Ser., 314, 759
Gopal-Krishna, Wiita P. J. 1991, ApJ, 373, 325
Grandi, P., Malaguti, G., & Fiocchi, M. 2006, ApJ, 642, 113
Guainazzi, M. 2008, Status of EPIC Calibrations, XMM-Newton SOC:ESAC, available at: `http://xmm2.esac.esa.int/docs/documents/CAL-TN-0018.pdf`
Guainazzi, M., Siemiginowska, A., Rodriguez-Pascual, P., & Stanghellini, C. 2004, A&A, 421, 461
Guainazzi, M., Matt, G., & Perola, G. C. 2005, A&A, 444, 119
Guainazzi, M., Siemiginowska, A., Stanghellini, C., et al. 2006, A&A, 446, 87
Gugliucci, N. E., Taylor, G. B., Peck, A. B., & Giroletti M. 2005, ApJ, 622, 136
Gupta, N., & Saikia, D. J. 2006, MNRAS, 370, 738
Gupta, N., Salter, C. J., Saikia, D. J., Ghosh , T., & Jeyakumar, S. 2006, MNRAS, 373, 972
Hardcastle, M. J., & Worrall, D. A. 2000, MNRAS, 314, 969
Hardcastle, M. J., Evans, D. A., & Croston, J. H. 2006, MNRAS, 370, 1893
Heckman, T. M., Ptak, A., Hornschemeier, A., & Kauffmann, G. 2005, ApJ, 634, 161
Holt, J., Tadhunter, C. N., & Morganti, R. 2003, MNRAS, 342, 227
Kalberla, P. M. W., Burton, W. M., Hartmann, D., et al. 2005, A&A, 440, 775
Isobe, T., Feigelson, E. D., & Nelson, P. I. 1986, ApJ, 306, 490
Labiano, A., O'Dea, C., Gelderman, R., et al. 2005, A&A, 436, 493
Labiano, A., O'Dea, C., Barthel, P. D., de Vries, W. H., & Baum, S. A. 2008, A&A, 477, 491
Laing, R. A., Jenkins, C. R., Wall, J. V., & Unger, S. W. 1994, in The First Stromlo Symposium: The Physics of Active Galactic Nuclei, ed. G. V. Bicknell, M. A. Dopita, & P. A. Quinn, ASP Conf. Ser., 54, 201
Lister, M. 2003, ASPC, 300, 71
Liu, X., Fuo, W.-F., Shi, W.-Z., & Song, H.-G. 2007, A&A, 470, 97
Magdziarz, P., & Zdziarski, A. A. 1995, MNRAS 273, 837
Marecki, A., Barthel, P. D., Polatidis, A., & Owsianik, I. 2003, PASA, 20, 16
Maiolino, R., Salvati, M., Bassani, L., et al. 1998, A&A, 338, 781
Mazzarella, J. M., Bothun, G. D., & Boroson, T. A. 1991, AJ, 101, 2034
Morrison, R., & McCammon, D. 1983, ApJ, 270, 199
Murgia, M. 2003, PASA, 20, 19
O'Dea, C. 1998, PASP, 110, 493
O'Dea, C., Baum, S. A., & Stanghellini, C. 1991, ApJ, 380, 66

O'Dea, C., Stanghellini, C., Baum, S., & Charlot, S. 1996, ApJ, 470, 806
O'Dea, C., de Vries, W. H., Worrall, D. M., Baum, S., & Koekmoer, A. 2000, AJ, 119, 478
O'Dea, C., Mu, B., Worrall, D. M., et al. 2006, ApJ, 653, 1115
Osterbrock, D. E. 1977, ApJ, 215, 733
Ostorero, L., Moderski, R., Stawarz, Ł, et al. 2009, AN, 330, 275
Phillips, R. B., & Shaffer, D. B. 1983, ApJ, 271, 32
Piconcelli, E., Bianchi, S., Miniutti, G., et al. 2008, A&A, 480, 671
Pihlström, Y. M., Conway, J. E., & Vermeulen, R. C. 2003, A&A, 404, 871
Polatidis, A. G., & Conway, J. E. 2003, PASA, 20, 69
Readhead, A. C. S., Taylor, G. B., Pearson, T. J., & Wilkinson, P. N. 1996, ApJ, 460, 634
Risaliti, G. 2002, A&A, 386, 379
Sambruna, R., Eracleous, M., & Mushotzky, R. 1999, ApJ, 526, 60
Schoenmakers, A. P., de Bryun, A. G., Röttgering, H. J. A., & van der Laan, H. 1999, A&A, 341, 44
Scheuer, P. A. G. 1974, MNRAS, 166, 513
Schmitt, J. H. M. M. 1985, A&A, 293, 178
Siemiginowska, A., Bechtold, J., Aldcroft, T. L., et al. 2002, ApJ, 570, 543
Siemiginowska, A., Stanghellini, C., Brunetti, G., et al. 2003, ApJ, 595, 643
Siemiginowska, A., Cheung, C. C., LaMassa, S., et al. 2005, ApJ, 632
Siemiginowska, A., LaMassa, S., Aldcroft, T. L., Bechtold, J., & Elvis, M. 2008, 684, 811
Spergel, D. N., Bean, R., Doré, O., et al. 2007, ApJS, 170, 377
Stanghellini, C. 2006, in Proceedings of the 8th VLBI Network Symposium, ed. A. Marecki et al., 18
Stanghellini, C., Baum, S. A., O'Dea, C. P., & Morris, G. B. 1990, A&A, 233, 379
Stanghellini, C., O'Dea, C. P., Baum, S. A., et al. 1997, A&A, 325, 953
Stanghellini, C., O'Dea, C. P., Dallacasa, D., et al. 1998, A&AS, 131, 303
Stanghellini, C., O'Dea, C. P., & Murphy, D. W. 1999, A&ASS, 134, 309
Stawarz, Ł., Ostorero, L., Begelman, M. C., et al. 2008, ApJ, 680, 911
Strüder, L., Briel, U., Dannerl, K., et al. 2001, A&A, 365, L18
Turner, M. J. L., Abbey, A., Arnaud, M., et al. 2001, A&A, 365, L27
Vermeulen, R. C., Pihlström, Y. M., Tschager, W., et al. 2003, A&A, 404, 861
Véron-Cetty, M.-P., & Veron, P. 2006, A catalogue of quasars and active nuclei: 12th edition
Vink, J., Snellen, I., Mack, K.-H., & Schillizzi, R. 2005, MNRAS, 367, 928
Voges, W., Aschenbach, B., Boller, T., et al. 1999, A&AS, 349, 389
White, R.-L., Becker, R.-H., Helfand, D.-J., & Gregg, M.-D. 1997, ApJ, 475, 479
Xiang, L., Dallacasa, R., Cassaro, P., Jiang, D., & Reynolds, C. 2005, 434, 123